Research Article
Journal of Advanced Development in Engineering and Science
Vol.15 ● No.44 • September – December 2025

Investigated Properties of Ceo_2 Doped Y257 Superconductors

Suppanyou Meakniti[1], Sujittra Sangchaisee[2], Paphassara Thipbanpot[2] and Thitipong Kruaehong[3*]

Received: 18 July 2025
Revised: 29 August 2025
Accepted: 1 September 2025

ABSTRACT

Polycrystalline $Y_2Ba_5Cu_7O_{15-X}$ (Y257) samples doped with cerium oxide (CeO_2) at concentrations of x = 0, 0.05, 0.10, 0.15, and 0.20 were synthesized via the solid-state reaction method at a sintering temperature of 950 °C. X-ray diffraction analysis revealed a mixture of superconducting and non-superconducting phases. The dominant superconducting phase exhibited an orthorhombic crystal structure (space group Pmmm), while secondary phases included Y_2BaCuO_5 (Pbnm), $BaCuO_2$ (Im-3m), and $Ba_2Cu_3O_6$ (Pccm). The fraction of the superconducting phase increased with CeO_2 content. Rietveld refinement indicated a slight expansion along the c-axis with increasing cerium doping. SEM imaging showed porous microstructures, while EDX mapping confirmed uniform elemental distribution. Electrical resistivity measurements using the four-probe method demonstrated a gradual increase in critical temperature (T_c) from 89.3 K (undoped) to 93.6 K (x = 0.20), consistent with values for Y123-type superconductors. These findings indicate that CeO_2 doping enhances the superconducting phase and improves the critical temperature of Y257 compounds.

Keywords: Superconductor; Solid state method; Critical temperature; Cerium doped

[1]General Science Program, Faculty of Education, Suratthani Rajabhat University, Suratthani, Thailand 84100
[2]Science Center, Faculty of Science and Technology, Suratthani Rajabhat University, Suratthani, Thailand 84100
[3]Department of Industrial Electrics, Faculty of Science and Technology, Suratthani Rajabhat University, Suratthani, Thailand 84100
*Corresponding author e-mail: thitipong.kru@sru.ac.th

Introduction

Since the discovery of the high-temperature superconductor La214 with a critical temperature of 35 K in 1986 [1], significant research has been conducted on ceramic superconductors with transition temperatures above the boiling point of liquid nitrogen. One of the most well-known compounds, $YBa_2Cu_3O_{7-x}$ (Y123), has a critical temperature of approximately 93 K [2] and has been developed into wires and tapes with high critical current density at 77 K. Since then, numerous Y-based superconductors have been synthesized, including $YBa_2Cu_4O_8$ (Y124) [3], $Y_2Ba_4Cu_7O_{15}$ (Y247) [4], and $Y_3Ba_5Cu_8O_{18}$ (Y358) [5], with critical temperatures ranging from 30 K to over 100 K, depending on oxygen content and structural variations. In 2010, Udomsamuthirun et al. [6] proposed a structural relationship where the sum of Y and Ba atoms equals the number of Cu atoms, linking the number of CuO_2 planes and Cu-O chains to atomic composition. Based on this principle, Kruaehong synthesized a novel Y-based superconductor, Y257 ($Y_2Ba_5Cu_7O_{15-x}$) [7], which exhibited a critical temperature of approximately 93 K and an orthorhombic crystal structure with lattice parameters a = 3.8108 Å, b = 3.8544 Å, and c = 26.4967 Å. Improving the superconducting properties of such materials, particularly critical current density (J_c) and critical magnetic field (H_c), often involves the incorporation of secondary phases. The inclusion of Y211 (Y_2BaCuO_5) is known to enhance flux pinning and increase J_c [8]. Other elements such as Pt [9], Sn [10], and $BaCeO_3$ [11] have been studied for their impact on microstructure and superconducting performance. In particular, cerium oxide (CeO_2) has been shown to improve intergranular connectivity and critical temperature in Y123-based superconductors [12]. Cerium oxide (CeO_2) has been widely investigated because of its unique redox capability associated with the Ce^{3+}/Ce^{4+} transition and its ability to create oxygen vacancies, which strongly influence both catalytic and electronic behaviors. These properties have made CeO_2 highly attractive in various fields, ranging from catalysis and energy storage to biomedical applications. In the context of high-temperature superconductors, the incorporation of CeO_2 as a dopant is particularly significant since oxygen vacancies and redox flexibility can directly affect grain connectivity, flux pinning, and overall superconducting performance. Therefore, exploring the role of CeO_2 in $Y_2Ba_5Cu_7O_{15-\delta}$ (Y257) provides a promising strategy to enhance the physical properties and stability of these superconducting materials [13].

In this study, we investigate the physical properties of Y257 ($Y_2Ba_5Cu_7O_{15-x}$) doped with various concentrations of cerium oxide (x = 0, 0.05, 0.10, 0.15, and 0.20). Samples were synthesized using the solid-state reaction method and characterized for phase composition, microstructure, elemental distribution, and superconducting transition temperature.

Materials and Methods

Polycrystalline samples of $Y_2Ba_5Cu_7Ce_xO_{15-x}$ with cerium concentrations of x = 0, 0.05, 0.10, 0.15, and 0.20 were synthesized by the solid-state reaction method. Starting materials included high-purity (99.99%) Y_2O_3, $BaCO_3$, CuO, and CeO_2 powders. Stoichiometric amounts were thoroughly mixed in an agate mortar and calcined at 950 °C for 24 hours in air, repeated twice to ensure homogeneity. The calcined powders were reground and pressed into cylindrical pellets (25 mm diameter, 3 mm thickness).

The pellets were sintered in a horizontal tube furnace at 950 °C for 24 hours, followed by slow cooling to 500°C and annealing for 12 hours in air. Phase identification was carried out using powder X-ray diffraction (XRD) in the 2θ range of 10° to 90°, and Rietveld refinement was employed for lattice parameter analysis. Superconducting transition temperatures (onset and offset) were measured using the standard four-probe method in the temperature range of 77 K to 120 K. Microstructural and elemental analyses were performed using Scanning Electron Microscopy (SEM) and Energy Dispersive X-ray Spectroscopy (EDX) with elemental mapping.

Results and Discussion

Figure 1 presents the powder X-ray diffraction (XRD) patterns of the undoped and CeO_2 doped Y257 samples, confirming the polycrystalline nature of the synthesized materials. The diffraction patterns were analyzed using the Rietveld refinement method [14], and the results show that the primary superconducting phase adopts an orthorhombic crystal structure (space group Pmmm) with peaks corresponding to the Y123 phase.

The samples consisted of two distinct phases. The first and dominant phase was the superconducting phase, with the highest content observed in the undoped sample. Interestingly, the proportion of the superconducting phase increased with CeO_2 doping. Conversely, the second phase comprised non-superconducting secondary phases, including Y_2BaCuO_5 (Y211, space group Pbnm), $BaCuO_2$ (space group Im-3m), and $Ba_2Cu_3O_6$ (space group Pccm). In the undoped sample, the superconducting and non-superconducting phases were found in proportions of approximately 80% and 20%, respectively. As shown in Table 1, CeO_2 doping led to an increase in the superconducting phase fraction and a corresponding decrease in non-superconducting phases.

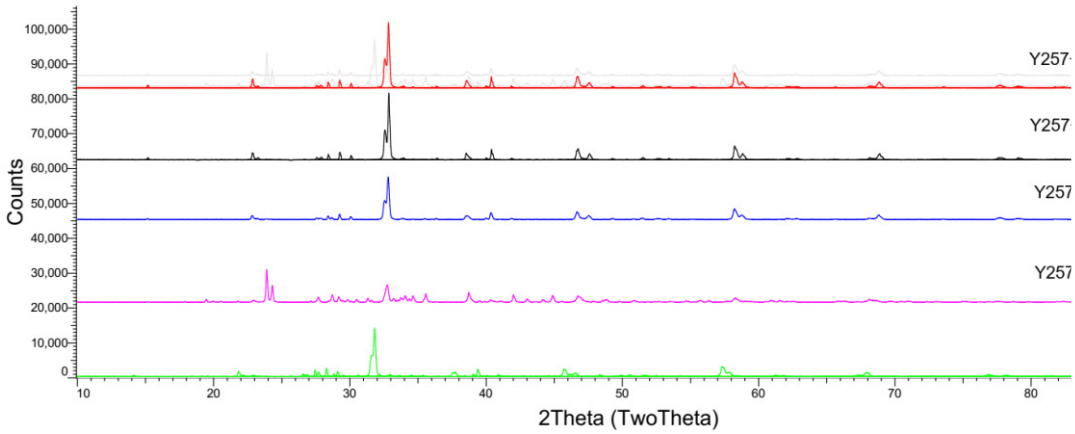

Figure 1 XRD patterns of the Y257 samples with varying CeO_2 doping.

Table 1 Percentages of the superconducting and non-superconducting phases in the Y257 samples.

Samples	Superconducting phase (%)	Non-superconducting phases (%)		
		Y_2BaCuO_5, Pbnm	$BaCuO_2$, Im-3m	$Ba_2Cu_3O_6$, Pccm
Y257	80	20	-	-
Y257+0.05Ce	87	-	6	7
Y257+0.10Ce	90	10	-	-
Y257+0.15Ce	92	8	-	-
Y257+0.20Ce	95	-	2	3

The lattice parameters of both the superconducting and non-superconducting phases, as presented in Tables 2 and 3, were determined using the Rietveld refinement method. The superconducting phase exhibited an orthorhombic crystal structure. For the undoped sample, the refined lattice parameters were a = 3.81975 Å, b = 3.88523 Å, and c = 26.68010 Å. Upon doping with CeO_2, a noticeable increase in the c-axis lattice parameter was observed, indicating lattice expansion with higher cerium content. As shown in Table 3, the non-superconducting phases were also characterized. The first secondary phase, Y_2BaCuO_5 (Y211), crystallized in the orthorhombic structure with the Pbnm space group. The second phase, $BaCuO_2$, exhibited a cubic structure corresponding to the Im-3m space group, while the third phase, $Ba_2Cu_3O_6$, showed an orthorhombic structure with the Pccm space group. All samples, regardless of CeO_2 content, contained both superconducting and non-superconducting phases. The presence

of non-superconducting phases is likely due to the high-temperature synthesis conditions used during sample preparation [15]. In addition, the refined lattice parameters of these non-superconducting phases (Table 3) reveal slight variations with CeO_2 doping. This suggests that the incorporation of Ce ions not only affects the superconducting $YBa_2Cu_3O_{7-\delta}$ matrix but also induces subtle structural modifications in the secondary phases. Such variations may influence phase stability, grain boundary formation, and ultimately the superconducting performance of the material. Therefore, the coexistence and interaction between superconducting and non-superconducting phases must be carefully considered when evaluating the role of CeO_2 addition in optimizing the microstructural and superconducting properties of Y257 samples.

Table 2 Lattice parameters of the superconducting phase ($Y_2Ba_5Cu_7O_{15-x}$).

Samples	lattice parameters		
	a(Å)	*b*(Å)	*c*(Å)
Y257	3.81975	3.88523	26.68010
	0.00004	0.00005	0.00013
Y257+0.05Ce	3.82093	3.88584	26.77332
	0.00005	0.00006	0.00014
Y257+0.10Ce	3.82020	3.88733	26.87624
	0.00007	0.00007	0.00022
Y257+0.15Ce	3.82364	3.88552	26.87762
	0.00009	0.00007	0.00022
Y257+0.20Ce	3.82432	3.88542	26.88885
	0.00013	0.00013	0.00085

Table 3 Lattice parameters of the non-superconducting phases present in the Y257 samples.

Samples	lattice parameters of the non-superconducting phases								
	a(Å)	*b*(Å)	*c*(Å)	*a*(Å)	*b*(Å)	*c*(Å)	*a*(Å)	*b*(Å)	*c*(Å)
Y257	12.17288	5.66052	7.14736	18.31059	18.31059	18.31059	13.04278	20.64500	11.42713
	0.00086	0.00043	0.00048	0.00018	0.00018	0.00018	0.00034	0.00043	0.00029
Y257+0.05Ce	12.18020	5.64675	7.14424	18.30278	18.30278	18.30278	13.02821	20.63465	11.43390
	0.00103	0.00059	0.00087	0.00018	0.00018	0.00018	0.00024	0.00035	0.00032
Y257+0.10Ce	12.19054	5.65528	7.12745	18.30574	18.30574	18.30574	13.03613	20.63683	11.42859
	0.00078	0.00035	0.00035	0.00022	0.00022	0.00022	0.00026	0.00037	0.00030
Y257+0.15Ce	12.18649	5.65848	7.12734	18.29214	18.29214	18.29214	13.04461	20.65713	11.44278
	0.00041	0.00014	0.00018	0.00022	0.00022	0.00022	0.00024	0.00037	0.00023
Y257+0.20Ce	12.13285	5.68731	7.15800	18.35197	18.35197	18.35197	13.04029	20.56614	11.41454
	0.00049	0.00044	0.00025	0.00524	0.00524	0.00524	0.00030	0.00048	0.00026

The surface morphology of the samples was examined using Scanning Electron Microscopy (SEM) with a magnification of 2,000x. The SEM images revealed that both undoped and CeO_2 doped Y257 superconductors exhibited inhomogeneous and porous surface textures. The surfaces typically displayed pebble-like grain morphology, which is a common feature of polycrystalline ceramic superconductors synthesized via solid-state reaction.

Figures 2 to 6 display the Scanning Electron Microscopy (SEM) images of the Y257 samples doped with varying concentrations of CeO_2, observed at a magnification of 2,000x. The micrographs reveal the characteristic surface morphology and grain structure of polycrystalline ceramic superconductors synthesized via the solid-state reaction method. In Figure 2, corresponding to the undoped Y257 sample, the surface appears inhomogeneous with irregularly shaped grains and a significant presence of pores. The grain boundaries are distinct, indicating weak intergranular connectivity, which is a common limitation in undoped high-temperature superconductors. As the CeO_2 doping level increases from 0.05 to 0.20 mol (Figures 3 to 6), a noticeable improvement in surface morphology is observed. The grain structure becomes more densely packed, and the porosity visibly decreases. The grains appear more uniformly distributed, with enhanced contact between adjacent grains. This microstructural evolution suggests improved grain growth and sintering, facilitated by the presence of cerium oxide during the thermal processing stage. The reduction in porosity and improved grain connectivity are crucial for enhancing the superconducting properties of the material. These improvements contribute to the increased critical temperature (T_c) and reduced weak-link behavior at grain boundaries. The SEM analysis thus supports the positive role of CeO_2 in promoting densification and enhancing the overall microstructural integrity of Y257 ceramics.

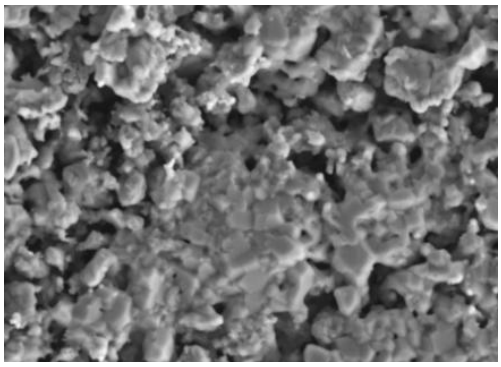

Figure 2 SEM micrograph of undoped Y257 at 2,000x magnification.

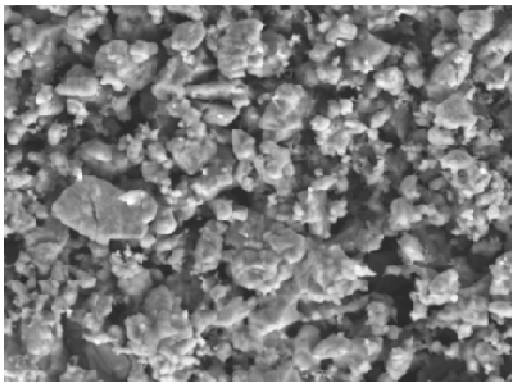

Figure 3 SEM micrograph of Y257 doped with 0.05 mol CeO_2.

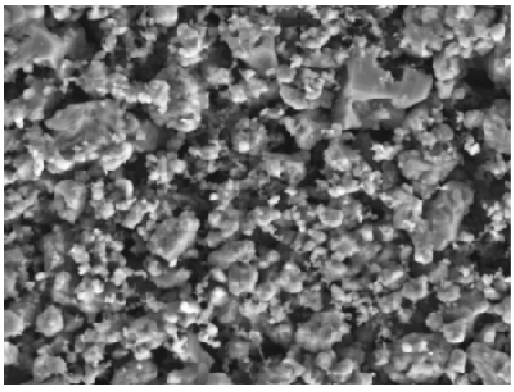

Figure 4 SEM micrograph of Y257 doped with 0.10 mol CeO_2.

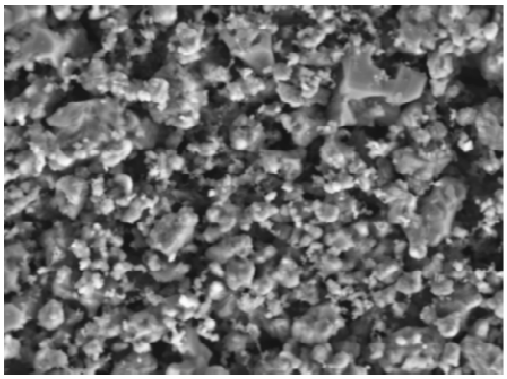

Figure 5 SEM micrograph of Y257 doped with 0.15 mol CeO_2.

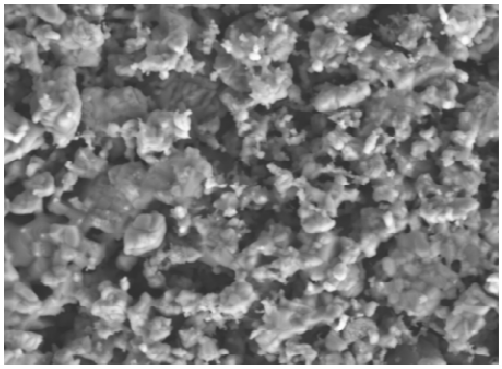

Figure 6 SEM micrograph of Y257 doped with 0.20 mol CeO_2.

Elemental analysis was performed using Energy Dispersive X-ray Spectroscopy (EDS) in mapping mode. The EDS maps showed that the undoped sample contained uniformly distributed elements of yttrium (Y), barium (Ba), copper (Cu), and oxygen (O). In CeO_2-doped samples, cerium (Ce) was also detected and found to be homogeneously distributed throughout the matrix, indicating successful incorporation of Ce into the Y257 structure.

Figures 7 to 11 present the Energy Dispersive X-ray Spectroscopy (EDS) elemental mapping results for the undoped and CeO_2-doped Y257 samples. The analysis was performed to investigate the spatial distribution of key elements within the samples and confirm the incorporation of Ce into the host matrix. In Figure 7, representing the undoped Y257 sample, the elements Y (yttrium), Ba (barium), Cu (copper), and O (oxygen) are uniformly distributed throughout the sample, indicating good compositional homogeneity.

This uniform distribution confirms that the solid-state reaction method effectively produced a well-mixed ceramic material. In the CeO_2-doped samples (Figures 8 to 11), the elemental maps clearly show the presence of cerium (Ce) in addition to Y, Ba, Cu, and O. Cerium is evenly distributed across the sample surface, with no observable clustering or phase segregation. This homogeneity suggests successful substitution or incorporation of Ce into the Y257 crystal lattice or at interstitial sites, without forming Ce-rich secondary phases. The uniform distribution of Ce supports the hypothesis that cerium doping enhances the superconducting phase content and improves grain connectivity. These EDS results are consistent with the observed increase in critical temperature and superconducting performance with higher CeO_2 concentrations.

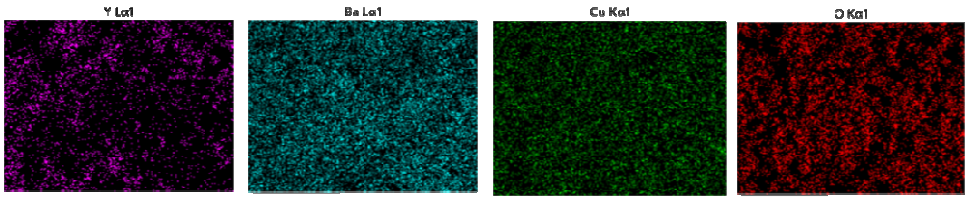

Figure 7 EDX elemental mapping of undoped Y257.

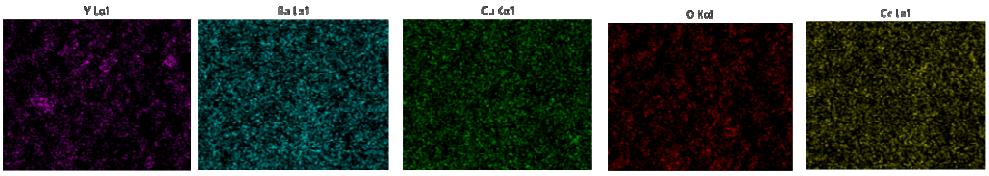

Figure 8 EDX mapping of Y257+0.05Ce.

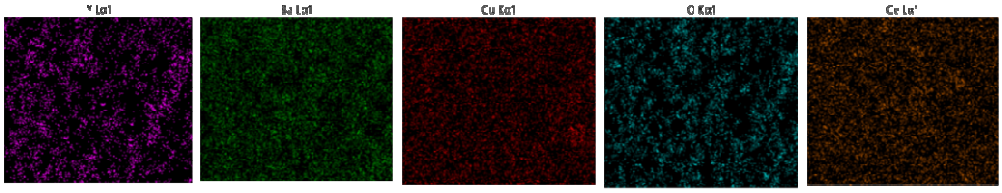

Figure 9 EDX mapping of Y257+0.10Ce.

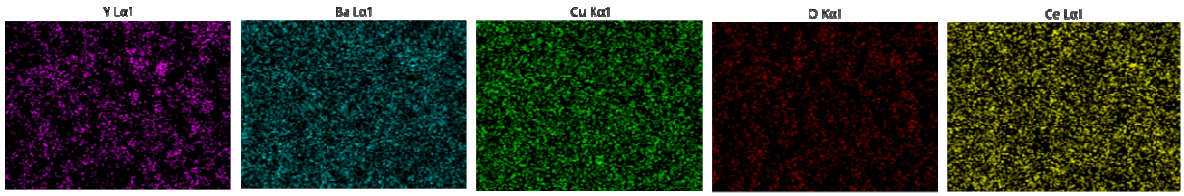

Figure 10 EDX mapping of Y257+0.15Ce.

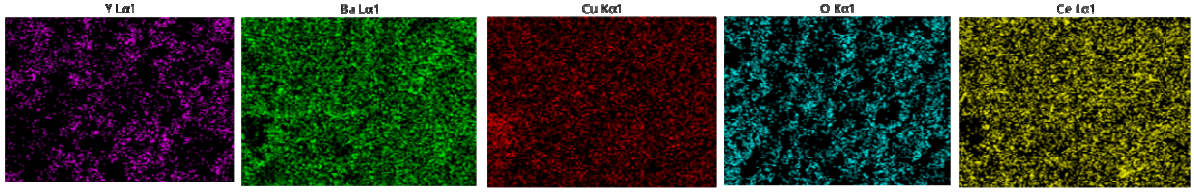

Figure 11 EDX mapping of Y257+0.20Ce.

The critical temperatures of the samples were determined using the standard four-probe resistivity measurement technique. For the undoped Y257 sample, the onset critical temperature (T_c onset) and offset critical temperature (T_c offset) were found to be 92.65 K and 85.98 K, respectively. With the introduction of CeO_2 doping, a gradual increase in both T_c onset and T_c offsetwas observed, indicating a positive effect of cerium content on the superconducting transition. Specifically, the average critical temperature increased from 89.35 K in the undoped sample to 93.6 K at a doping level of x = 0.20)as shown in Table .(4

Table 4 presents the onset and offset critical temperatures for all samples. The onset critical temperature is defined as the temperature at which the sample begins to deviate from the normal resistive state, while the offset critical temperature corresponds to the temperature at which zero resistivity is achieved. The difference between these two temperatures (ΔT_c) provides insight into the transition width and superconducting homogeneity of the material. An increase in ΔT_c with higher CeO_2 content suggests improved grain connectivity but also indicates the possible presence of minor non-superconducting secondary phases. CeO_2 doped Y257samples exhibit enhanced superconducting properties, with higher average critical temperatures and broadened transition widths [16]. All samples show T_c values within the typical range for $YBa_2Cu_3O_{-7x}$ (Y(123, around 93K, confirming that CeO_2 doping can effectively improve the superconducting performance of Y257 ceramics.

Table 4 lists the onset and offset critical temperatures for each sample.

Samples	T_c offset (K)	T_c onset (K)	ΔT_c	T_c average
Y257	85.98	92.65	6.67	89.315
Y257+0.05Ce	87.35	93.47	6.12	90.410
Y257+0.10Ce	87.49	95.65	8.16	91.570
Y257+0.15Ce	88.32	96.41	8.09	92.365
Y257+0.20Ce	89.35	97.94	8.59	93.645

Conclusion

Cerium-doped Y257 ($Y_2Ba_5Cu_7Ce_xO_{15-x}$) superconductors were successfully synthesized by the solid-state reaction method. XRD and Rietveld refinement confirmed the presence of an orthorhombic superconducting phase and secondary non-superconducting phases. Increasing CeO_2 content led to a higher fraction of the superconducting phase and a slight expansion of the c-axis lattice parameter. SEM and EDX analyses showed porous microstructures and homogeneously distributed elements. Electrical measurements revealed a progressive increase in critical temperature with cerium doping, maintaining values within the range typical of Y123 superconductors. These results demonstrate that CeO_2 doping can enhance the superconducting performance of Y257 compounds.Building on these findings, a potential avenue for further improving superconducting properties is through additional CeO_2 doping, which may introduce more flux pinning centers and further increase the critical current density (J_c) and critical magnetic field (H_c). Future studies exploring this approach could provide practical strategies for enhancing Y257 superconductors.

Acknowledgments

The authors would like to express their sincere gratitude for the financial support received from the Research and Development Institute of Suratthani Rajabhat University and the Fundamental Fund in 2025.

References

[1] Bednorz, J. G., & Müller, K. A. (1986). Possible High T_c Superconductivity in the Ba-La-Cu-O System. *Zeitschrift für Physik B Condensed Matter*, 64, 189–193.

[2] Wu, M. K., et al. (1987). Superconductivity at 93 K in a New Mixed-Phase Y-Ba-Cu-O Compound System at Ambient Pressure. *Physical Review Letters*, 58(9), 908–910.

[3] Marsh, P., et al. (1988). Crystal Structure of the 80 K Superconductor $YBa_2Cu_4O_8$. *Nature*, 334, 141–143.

[4] Bordet P, et al. (1988). Structure Determination of the New High Temperature

Superconductor $Y_2Ba_4Cu_7O_{14+x}$. *Nature*, 334, 596–598.

[5] Aliabadi, A., et al. (2009). A New Y-Based HTSC with T_c Above 100 K. *Physica C: Superconductivity and Its Applications*, 469(22), 2012–2014.

[6] Udomsamuthirun, P., et al. (2010). The New Superconductors of YBaCuO Materials. *Journal of Superconductivity and Novel Magnetism*, 23, 1377–1380.

[7] Kruaehong, T. (2013). Preparation and Characterization of the New Y257 Superconductors. *Advanced Materials Research*, 770, 22–25.

[8] Ouerghi, A., et al. (2017). The Influence of Slow Cooling on Y211 Size and Content in Single-Grain YBCO Bulk Superconductor Through the Infiltration-Growth. *Physica C: Superconductivity and Its Applications*, 534, 37–44.

[9] Chow, J. C. L., et al. (1998). Effects of Pt Doping on the Size Distribution and Uniformity of Y_2BaCuO_5 Particles in Large-Grain YBCO. *Superconductor Science and Technology*, 11(4), 369–374.

[10] Choi, S. M., et al. (2013). Flux Pinning Characteristics of Sn-Doped YBCO Film by the MOD Process. *Physica C: Superconductivity and Its Applications*, 485, 154–159.

[11] Mahmood, A., et al. (2009). Improvement of the Superconducting Properties of an Infiltrated YBCO Bulk Superconductor by a $BaCeO_3$ Addition. *Physica C: Superconductivity and Its Applications*, 469(15-20), 1165–1168.

[12] Polovkova, J., et al. (2009). Structural and magnetization properties of Ce doped $YBa_2Cu_3O_{7-\delta}$. In *7th International Conference on measurement* (p. 266–269). 20-23 May, 2009, Smolenice, Slovakia.

[13] Xu, C., & Qu, X. (2014). Cerium Oxide Nanoparticle: A Remarkably Versatile Rare Earth Nanomaterial for Biological Applications. *NPG Asia Materials*, 6(3), e90.

[14] Carvajal, J. (2001). *An Introduction to the Program FULLPROF*. Saclay: Laboratoire Léon Brillouin.

[15] Diko, P., et al. (2008). Microstructure of YBCO Bulk Superconductors with CeO_2 Addition. *Materials Science and Engineering: B*, 151(1), 7–10.

[16] Inoue, K., et al. (2017). Effect of Carbon Nanotube Addition on Superconductivity in Y-Ba-Cu-O Bulk Superconductors. *Journal of Physics: Conference Series*, 871, 012002.